

Supplementary Information: Harnessing bistability for directional propulsion of soft, untethered robots

Bistable Mechanism Analysis. In order to analyze the bistable mechanism, we first fabricate a bistable mechanism-muscle pair enclosed in a planar shell identical to that of a single stroke swimming robot (Supp. Fig. 1.a and Movie S8). The four bars within the bistable mechanism form two “V” shapes pointing to the right, representing one of the stable states of the mechanism. The sample (the pair confined in the planner shell) is then immersed in 60 °C water (state I), equivalent to the glass transition temperature of the muscle material (VeroWhitePlus). As the muscle temperature rises due to water contact, both of the deformed beams within the muscle start relaxing into their original/printed shape. At the onset of the instability, where the truss-like bars of the bistable mechanism are vertical (state II), the muscle pushes the mechanism slightly towards its second stable state (where the “V” shapes are pointing to the left) (state III).

In order to model the bistable behavior of the mechanism, we now consider one of its four bars (Supp. Fig. 1.b). The bars are printed with VeroWhitePlus with Young’s modulus $E = 2 \times 10^9$ Pa, while its connections to the planar shell are printed with Aguils300 with a Young’s modulus $E = 2 \times 10^6$ Pa. Since the bar material has a stiffness that is 10^3 higher than its connection points, we model the bar as an inclined rigid truss element (Supp. Fig. 1.c) supported by two torsional springs with a spring constant (k_θ) and a linear spring with a constant (k) (Supp. Fig. 1.c). The rotational springs k_θ are the torsional resistance of the compliant joints. The linear spring, k simulates bending of the flexible support through linear force in the y direction.

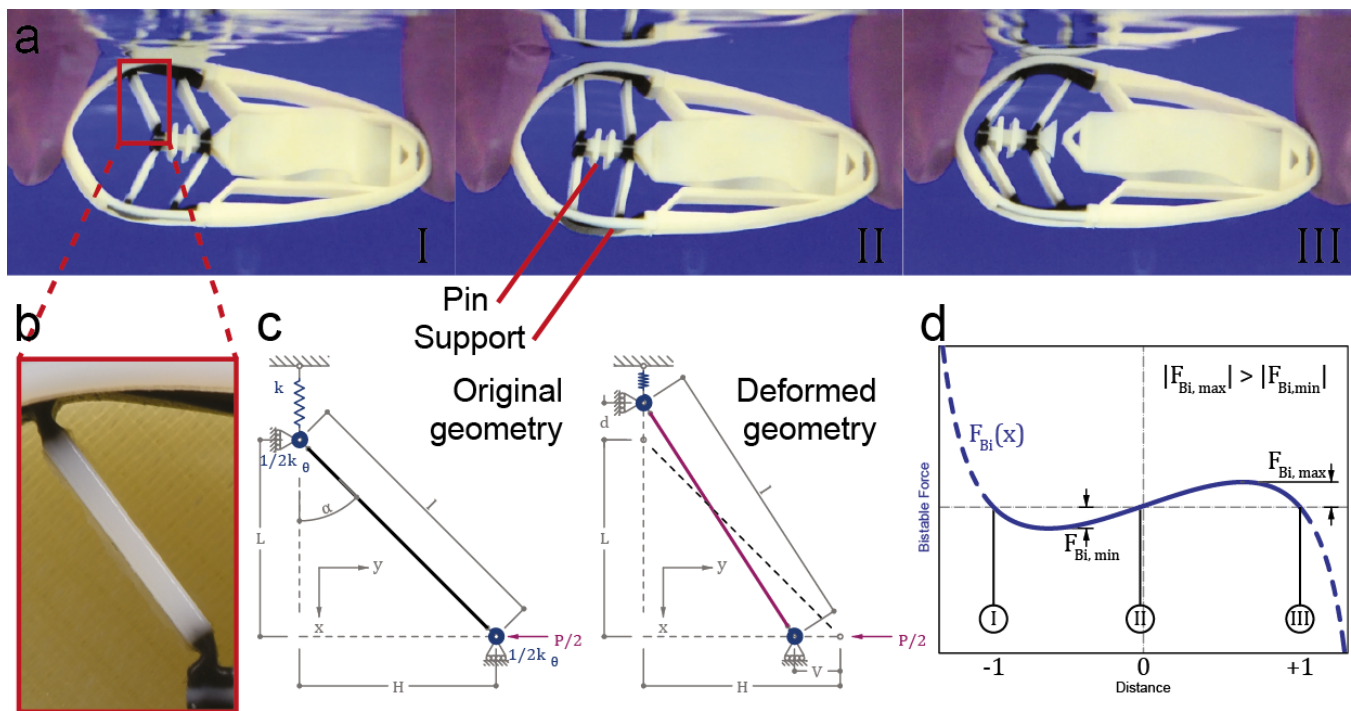


Fig. 1. a. Video snapshot of the actuation of the bistable mechanism. Note that from stage II to III, the shape memory polymer does not contribute to propulsion. b. A zoom in view of the bistable truss geometry, the black regions represent the flexible material, and the white is the rigid material. c. An idealization of the truss geometry in both the original and the deformed state. The support is idealized by a linear spring k , and the joints by a torsional spring k_θ . d. The force displacement relationship of the bistable mechanism as derived in equation 5.

We use a Lagrangian equation to construct a relationship between the force P and the corresponding displacement V with respect to the deformed geometry. The bar is assumed to be axially rigid.

$$\mathcal{L} = \frac{1}{2}kd^2 + \frac{1}{2}k_\theta\Delta\alpha^2 - \frac{1}{2}PV \quad [1]$$

Then we consider the deformed geometry with a rigid truss bar, to relate the different displacements in the model:

$$\sqrt{H^2 + L^2} = \sqrt{(H - V)^2 + (L + d)^2} \quad [2]$$

The solution of d is the difference between the deformed projected length and the original one,

$$d = \sqrt{2HV + L^2 - V^2} - L \quad [3]$$

To simplify the representation, we denote the first term of the solution as

$$L_1 = \sqrt{2HV + L^2 - V^2}.$$

The Lagrangian equation becomes

$$\mathcal{L} = \frac{1}{2}k(L_1 - L)^2 + \frac{1}{2}k_\theta \left(\arctan \frac{H - V}{L_1} - \arctan \frac{H}{L} \right)^2 - \frac{1}{2}PV \quad [4]$$

We obtain the relationship between P and V , by differentiating the system w.r.t. to V and setting the result to zero, $\frac{\partial \mathcal{L}}{\partial V} = 0$. Such an equation provides the means to assess the impact each variable on the overall behavior of the system has, and therefore design the bistable mechanism.

$$P = -2\frac{1}{L_1} [k(L - L_1)(H - V) + k_\theta \left(\arctan \left(\frac{H - V}{L_1} \right) - \arctan \left(\frac{H}{L} \right) \right)] \quad [5]$$

In the initial state (I), The shape memory muscle doesn't exert any force $P = 0$ on the bistable mechanism (Supp. Fig. 1.d). As the surrounding water heats the muscle, it starts to relax to its original/printed shape, pushing the bistable truss towards its second stable state. Until the muscle pushes the truss to be vertical, i.e. $H = 0$ (II), beyond this point, the mechanism flips to the second equilibrium state (III), where the muscle is physically detached from the mechanism.

Material characterization and Simulation. The materials utilized in this study (Agilus30, FLX9895, VeroWhitePlus or RGD835, high temperature resistant material or RGD525) are characterized using Differential scanning calorimetry (DSC) to determine their glass transition temperature. VeroWhitePlus is used as the SMP muscle for all presented robots. FLX9895 is used in conjunction with VeroWhitePlus in the Cargo Deployment example. For both of these SMPs, two further sets of material data are obtained, 1) the fully relaxed modulus, and 2) frequency sweeps of the storage modulus at different temperatures. The fully relaxed modulus is obtained using an Instron E3000 dynamic testing machine with a 3 kN load cell and a temperature insulation chamber. The experiments are performed at 80 °C with a rate of 0.05 mm s⁻¹. Cylindrical specimens with a diameter of 7 mm and height of 9 mm are used. The storage modulus is obtained using a dynamic mechanical analysis (DMA) (Mettler Toledo DMA 861) machine. Specimens (3.00 mm × 4.30 mm × 2.05 mm) are tested under oscillatory shear (frequency: 0.01 to 100 Hz, amplitude: 0.5 μm). The test is conducted for temperatures 20, 40, 50, 60, 80, and 100 °C for VeroWhitePlus and -40, -17, 2, 12, 21, 30, 40, 49 °C for FLX9895.

We assume a time-temperature superposition principle, where the behavior of the material at a given temperature can be modeled as multiplication of the relaxation times at a reference temperature T_{ref} and the shift factors at that temperature (Eq. 6).

$$\tau_i(T) = a_T \tau_i(T_{\text{ref}}) \quad [6]$$

The Williams-Landel-Ferry (WLF) equation (Eq. 7) is then used to approximate these shift factors a_T to construct a continuous storage modulus master curve at a reference temperature (275 K for FLX9895 and 313.15 K for VeroWhitePlus) (1).

$$\log_{10} a_T = \log_{10} \frac{\tau(T)}{\tau(T_{\text{ref}})} = -\frac{C_1(T - T_{\text{ref}})}{C_2 + (T - T_{\text{ref}})}, \quad T > T_{\text{ref}} \quad [7]$$

Fourier transform is then used to translate the storage modulus to a relaxation modulus which is needed as an input for Abaqus (Eq. 8) (1).

$$G(t) = G_\infty + \frac{2}{\pi} \int_0^\infty \left[\frac{G' - G_\infty}{\omega} \right] \sin \omega t d\omega \quad [8]$$

The Prony series is constructed using an approximation of equation 8 with 11 fitted coefficients (2). The constructed Prony series has 19 and 29 non-equilibrium branches for VeroWhitePlus and FLX9895 respectively. The Prony series and the temperature-time shift (TRS) coefficients are listed for both materials in Supplementary table 1 and 2.

$$G(t) = G_\infty + \sum_{i=1}^N G_i e^{-t/\tau_i} \quad [9]$$

The resulting FEM simulations of the SMP muscle of the heating, programming, cooling, and reheating cycles are presented in (Supp. Fig. 2). First, in a heated condition i.e., prescribed temperature ($T \geq T_g$), with a ramping in the prescribed displacement (Region A). The calculated corresponding force increases to its maximum. Second, in Region B, the prescribed displacement is kept constant while the prescribed temperature decreases to below T_g . Third, only the constraint on displacement is removed, i.e., no prescribed displacement. A slight rebound in displacement is observed (Region C) both in simulations and in experiments. Finally, in Region D, the prescribed temperature is increased to T_g and the SMP muscle relaxes to its original shape. The maximum force observed during the simulation is recorded for each SMP muscle, and plotted in Figure 2 against the measured maximum force from the experiments.

Table 1. Prony series of VeroWhitePlus and FLX9895 as implemented in Abaqus

VeroWhitePlus		FLX9895	
τ_i	G_i	τ_i	G_i
2.84E-06	0.047085	2E-09	0.037155
3.01E-05	0.047839	1E-08	0.036325
0.000215	0.021854	5E-08	0.019428
0.000214	0.039146	1E-07	0.036963
0.006686	0.046696	5E-07	0.025824
0.002274	0.060725	0.000001	0.048254
0.030904	0.078175	0.000005	0.029066
0.17528	0.079955	0.00001	0.061186
0.63842	0.05944	0.00005	0.047911
2.7039	0.11531	0.0001	0.048443
17.23	0.095187	0.0005	0.046758
58.742	0.039878	0.001	0.081033
134.64	0.097911	0.005	0.088524
996	0.10801	0.01	0.069187
10000	0.043986	0.05	0.11156
100000	0.012053	0.1	0.043557
1000000	0.001282	0.5	0.079339
10000000	0.000943	1	0.023205
50000000	0.000521	5	0.038059
		10	0.004878
		50	0.015653
		100	5.27E-14
		500	0.003613
		1000	0.000806
		5000	0.001064
		10000	0.000212
		50000	0.00029
		100000	0.000218
		1000000	0.000239

Table 2. TRS coefficients as input in Abaqus for both VeroWhitePlus and FLX9895

	VeroWhitePlus	FLX9895
T_{ref}	313.15	275.00
C_1	21.5657	19.987
C_2	97.4544	109.53

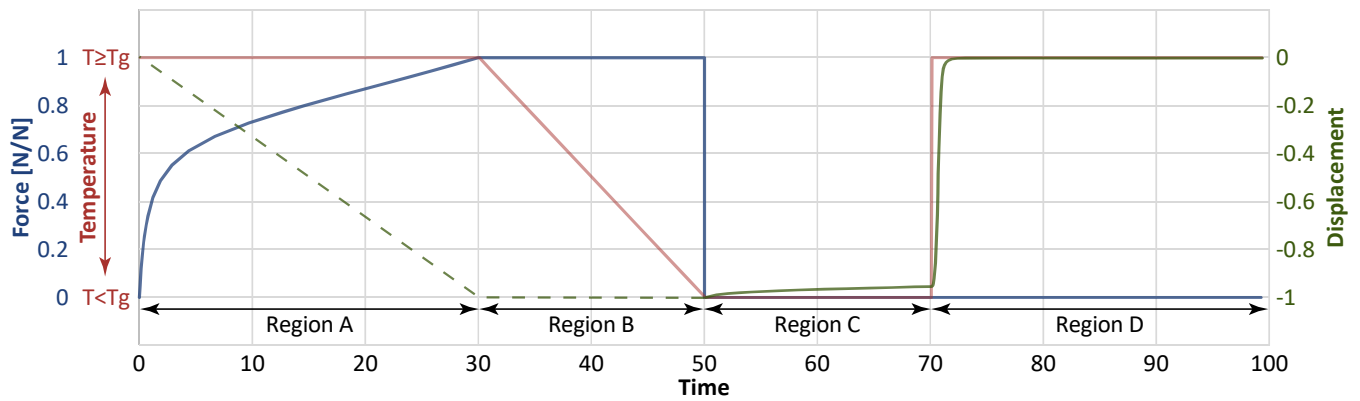


Fig. 2. Finite element simulations of the SMP muscle showing force, displacement and the corresponding ambient temperature. In Region A, the SMP muscle is programmed using a prescribed displacement under high temperature. The corresponding force is measured. In Region B, the displacement is kept constant as the system is cooled to below the glass transition temperature. In Region C, the prescribed displacement is removed, which shows that the programmed shape remains unaltered at a cold temperature. In Region D, the temperature is increased, and the SMP muscle recovers to its printed shape.

The role of bistability vs muscles in propulsion. In order to assess the contribution of the muscle-induced force on the distance traveled by the swimming robot, we deploy the same robot with various muscles. We systematically increase the thickness of the beams within the muscle, therefore increasing the resultant force (Supp. Fig. 3.a). For beams with thickness < 1.2 mm, the robot did not move forward, as the muscle force is not strong enough to overcome the bistability energy barrier. All the muscles with beams > 1.2 mm overcame the energy barrier and were able to propel the robot forward. However, the robot traveled the same distance (Supp. Fig. 3.b), regardless of the increase of the force amplitude by a factor 2. Therefore, the distance traveled by the swimmer depends on the bistable element rather than the muscle force, as long as the muscle is strong enough to push the mechanism to the onset of the instability.

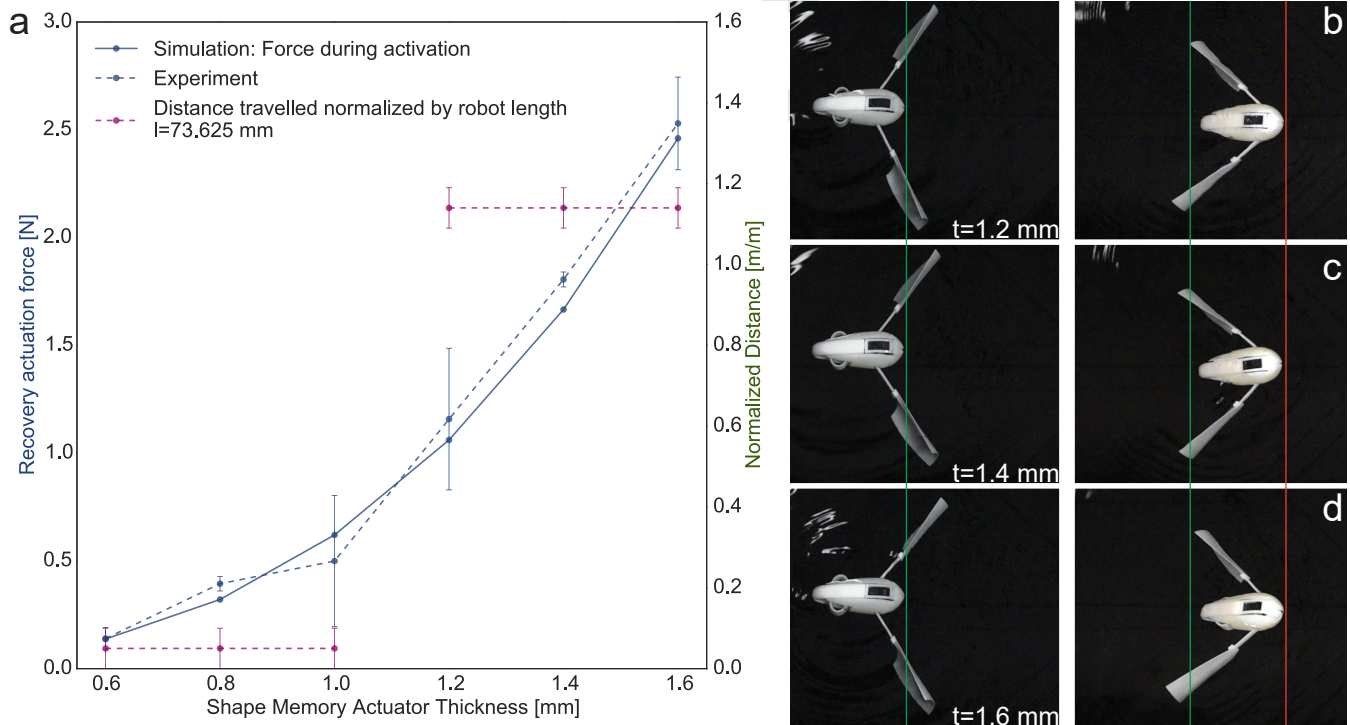


Fig. 3. Three swimmers travel the same distance when the shape memory actuator of three different beam thicknesses are used. This shows that propulsion comes predominantly from triggering of the bistable mechanism. The beam thickness values are 1.2, 1.4, 1.6 mm.

Movies.

SI Movie 1 Propulsion of a single stroke swimmer. The distance travelled is approximately $1.15l$ where l is the body length of the swimmer.

SI Movie 2 Shape memory muscle of different thickness exhibiting different time to activation.

SI Movie 3 Propulsion of a two-stroke swimmer. The sequence of activation is controlled by the thickness of the shape memory muscle. The distance traveled is approximately $1.9l$ (where l is the length of the single actuator swimmer).

SI Movie 4 Propulsion of a two-stroke directional swimmer. The programmed path is straight followed by a left turn. The distance traveled is approximately $0.5l$ after the first stroke, and a turn of 23.85° after the second stroke.

SI Movie 5 Propulsion of a two-stroke directional swimmer. The programmed path includes a left turn followed by a right turn. The rotation is approximately 21.64° after the first stroke, and -21.45° after the second stroke.

SI Movie 6 Shape memory muscle of different material exhibiting controlled activation depending on the surrounding temperature.

SI Movie 7 Propulsion of a reversing swimmer. The programmed operation includes a forward stroke, deployment of cargo, and a reverse stroke. The sequence of activation is controlled by the temperature of the surrounding environment. The first stroke is activated when water reaches T_L , deployment occurs when water is heated to T_H , then the reverse stroke occurs.

SI Movie 8 Internal mechanism of the actuator showing the shape memory muscle pushing the bistable mechanism from one equilibrium state to the next.

1. Ferry JD (1980) *Viscoelastic Properties of Polymers*. (John Wiley & Sons, Inc., Toronto), 3rd edition, pp. 1–672.

2. Schwarzl FR (1975) Numerical calculation of stress relaxation modulus from dynamic data for linear viscoelastic materials. *Rheologica Acta* 14(7):581–590.

DRAFT